NON-DESTRUCTIVE TESTING THEORETICAL STUDY ON SKIN TUMOR DETECTION USING LONG-PULSED INFRARED THERMAL WAVE TESTING TECHNOLOGY

by

Chiwen BU[a], Haijiang XU[a], Zeqing MAO[a], Dong ZHANG[a], and Chibin PU[b*]

[a] People's Hospital of Guanyun County, Lianyungang, China
[b] Department of Gastroenterology, Zhongda Hospital, Southeast University, Nanjing, China

Original scientific paper
https://doi.org/10.2298/TSCI180823204B

Skin cancer is one of the dangerous form of cancer spreading vigorously among humans, so its early detection is very important for further treatment. Theoretical study on skin tumor detection using long-pulsed infrared thermal wave testing technology (LP-ITWTT) has been carried out. The working principle of LP-ITWTT was described. The 3-D thermal model for skin tumor using LP-ITWTT was established and calculated. The effect of tumor geometry size including radius, depth and thickness to the measurement parameter C_{max} is studied, and the influence law has been got, which can provide a theoretical basis for the diagnosis of skin tumors using LP-ITWTT .

Key words: *skin tumor, geometry size, long-pulsed, thermal wave testing*

Introduction

Cancer has been a disease of mankind for many years, and it is more serious for the developed countries. Moreover, the World Health Organization predicts that by 2030, 27 million people in the world will have cancer. Among all, skin cancer is one of the dangerous form of cancer spreading vigorously among humans, so its early detection is very important for further treatment [1-4].

Based on the thermal effect theory of biological tissue, researchers have carried out the research of medical application of infrared technology and biomedical heat transfer, and formed the infrared medical thermal imaging technology (IMTIT). The IMTIT is an integrated technology of the combination of medical technology, infrared technology and computer multimedia technology, which can record the temperature field of human body. Compared with X-CT, MRI, ultrasound detection, IMTIT with high accuracy, no nuisance and high safety performance, can provide a new method for early diagnosis of human diseases. Godoy *et al.* [5] proposed dynamic thermal imaging with infrared cameras and achieved high levels of sensitivity and specificity by judiciously selecting pixels with the same initial temperature for skin cancer screening. Hagerlind *et al.* [6] investigated the usefulness of the combination of near infrared and skin impedance spectroscopy as a supportive tool in the diagnosis and evaluation of skin tumors in primary health care.

Theoretical study on skin tumor detection using long-pulsed infrared thermal wave testing technology (LP-ITWTT) has been carried out in this paper. First, the principle of

* Corresponding author, e-mail: 153670599@qq.com

LP-ITWTT is described. Then, 3-D thermal model for skin tumor using LP-ITWTT is built and effect of tumor geometry size and depth was discussed.

The principle of skin tumor using LP-ITWTT and the 3-D thermal model for skin tumor

The basic principle of skin tumor using LP-ITWTT is shown in fig. 1. Halogen lamps controlled by a light regulating device and function generator are used to emit long-pulsed heat flux. The tested skin specimen with a tumor is excited by the heat source, and an infrared camera is adopted to capture the thermal image sequence of the skin surface, which will be stored and processed by the computer with analysis software. Heat transfer in biological tissues is a complicated process that involves heat conduction, blood perfusion and metabolic heat generation. In this section, a 3-D thermal model for skin tumor detection using long-pulsed thermal wave testing technology is established. It is described as a mixed initial boundary value problem of partial differential equations of parabolic type. A skin model of 16 mm × 16 mm × 11.6 mm, which contains a discontinuity tumor is considered, and the structure size is shown in fig. 2 and tab. 1, [7].

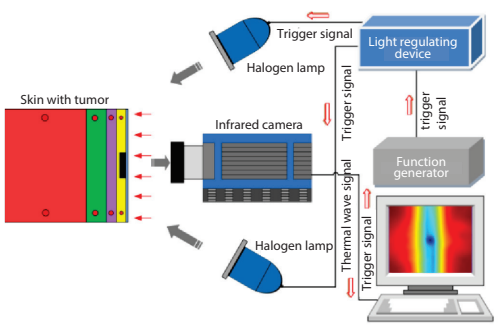

Figure 1. The basic principle of LP-ITWTT

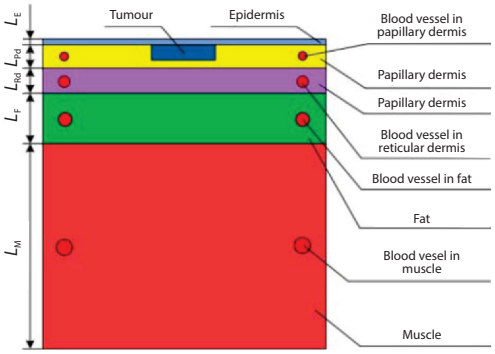

Figure 2. Structure of the skin model

Table 1. Geometrical parameters of the built skin model

Skin		W_1 [mm]	16
		W_2 [mm]	16
		L [mm]	11.6
Tissue layers	Epidermis	L_E [mm]	0.1
	Papillary dermis	L_{Pd} [mm]	0.7
	Reticular dermis	L_{Rd} [mm]	0.8
	Hypodermis	L_F [mm]	2
	Muscle	L_M [mm]	8
Blood vessel in tissue layers	Papillary dermis	d_{BvPd} [mm]	0.26
	Reticular dermis	d_{BvPd} [mm]	0.32
	Hypodermis	d_{BvF} [mm]	0.8
	Muscle	d_{BvM} [mm]	1.0
Tumour		r [mm]	0.2, 0.3, 0.4, 0.5, 0.6, 0.8, 1.0
		l [mm]	0.2, 0.3, 0.4, 0.7, 0.8
		h [mm]	0.1, 0.15, 0.35, 0.45, 0.5, 0.6, 0.75

In the model, the effects of the blood flow are treated as a temperature-dependent heat source, so Pennes bioheat equation [8-10] has been used as shown:

$$\rho c\frac{\partial T}{\partial t}=\lambda_x\frac{\partial^2 T}{\partial x^2}+\lambda_y\frac{\partial^2 T}{\partial y^2}+\lambda_z\frac{\partial^2 T}{\partial z^2}+q_{\mathrm{b}}+q_m \tag{1}$$

where ρ and c denote density and specific heat, respectively, λ_x, λ_y, λ_z – the thermal conductivities of tissue in the x-, y-, and z-directions, q_b – the heat transfer between the blood and biological tissues, and q_m – the metabolic heat generation.

It is assumed that the heat transfer between the blood and biological tissues q_b is proportional to the blood perfusion rate and the difference between arterial blood temperature and local tissue temperature, it can be expressed:

$$q_b=V\rho_b c_b\left(1-m\right)\left(T_a-T\right) \tag{2}$$

where V is blood perfusion rate of unit volume, ρ_b and c_b – the density and specific heat of blood, m – the thermal unbalance coefficient between biological tissue and blood and it is assumed 0, T_a – the supplying arterial blood temperature assumed constant, and T – the skin temperature. Let $\omega_b = V\rho_b$, which means blood perfusion rate. So eq. (1) can be expressed:

$$\rho c\frac{\partial T}{\partial t}=\lambda_x\frac{\partial^2 T}{\partial x^2}+\lambda_y\frac{\partial^2 T}{\partial y^2}+\lambda_z\frac{\partial^2 T}{\partial z^2}+\omega_b c_b(T_a-T)+q_m \tag{3}$$

In order to evaluate the surface temperature alteration induced by the presence of a tumour, the boundary conditions can be written:

$$-\lambda_x\frac{\partial T(x,y,z,t)}{\partial x}|_{x=H}=Q(t)+h_f\left[T_a-T(H,y,z,t)\right]+\sigma\varepsilon\left[T_a^4-T^4(H,y,z,t)\right] \tag{4a}$$

$$T(0,y,z,t)=T_c \tag{4b}$$

$$-\lambda_y\frac{\partial T(x,y,z,t)}{\partial y}|_{y=0}=-\lambda_y\frac{\partial T(x,y,z,t)}{\partial y}|_{y=W_1}=0 \tag{4c}$$

$$-\lambda z\frac{\partial T(x,y,z,t)}{\partial z}|_{z=0}=-\lambda_z\frac{\partial T(x,y,z,t)}{\partial z}|_{z=W_2}=0 \tag{4d}$$

The initial condition is:

$$T(x,y,z,t)|_{t=0}=T(x,y,z,0)=T_{\mathrm{c}} \tag{4e}$$

where $Q(t)$ is long pulsed heat flux, h_f – the convective heat transfer coefficient, h_f = 10 W/m^{2}K, T_a – the ambient temperature, and T_c – the core body temperature, T_c = 310 K. Thermal physical parameters for the various layers and blood vessels are shown in tab. 2.

Table 2. Thermal physical parameters [9]

Tissue	c [Jkg^{-1}K^{-1}]	λ [Wm^{-1}K^{-1}]	ρ [kgm^{-3}]	ω_b [s^{-1}]	q_{m} [Wm^{-3}]
Epidermis	3589	0.235	1200	0	0
Papillary dermis	3300	0.445	1200	0.0002	368.1
Reticular dermis	3300	0.445	1200	0.0013	368.1
Hypodermis	2674	0.185	1000	0.0001	368.1
Muscle	3800	0.51	1085	0.0027	684.2
Melanoma	3852	0.558	1030	–	–
Blood vessels	3770	0.501	1060	–	–

The effect of tumor geometry size and depth

The temperature distribution of skin surface with tumor

The heat transfer FEM simulations have been carried out for the built 3-D thermal model for skin tumor using LP-ITWTT. The tumor radius r = 0.5 mm, depth h = 0.5 mm, and thickness l = 0.7 mm. The skin surface is ex-cited with long pulsed heat flux power, which is set as 500 W for 120 seconds, and the solution time is set to 200 seconds with step by 1 second.

Figure 3. shows the temperature distribution of the skin surface at some moments after the long pulse excitation. From fig. 3, it can be seen that there are temperature differences between the normal regions and abnormal regions, and the heat flux transverse diffusion occurs gradually with the proceeding of heat conduction, so the tumor in the skin experiences the process of obscure, gradually clear, and gradually obscure.

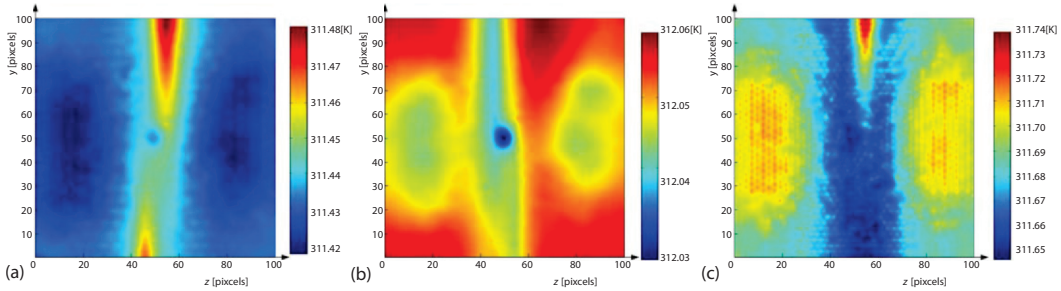

Figure 3. The temperature distribution of the skin surface at different moments; (a) t = 20 s, (b) t = 50 s, and (c) t = 80 s

In order to analyze the effect of the geometrical parameters of the tumor, systematic simulation has been done for 3-D thermal model with different geometrical size of the tumor. All the thermal images of the skin surface are normalized, and a measurement parameter called maximum contrast, c_{max}, is defined in eq. (5). Contrast is one of the indexes of infrared thermal wave non-destructive testing, which can reflect the detection ability of tumors, that is, the sensitivity of detection.

$$c_{\max} = T_{\text{normalization\_mean}} - T_{\text{normalization\_c}} \tag{5}$$

where $T_{\text{normalization\_mean}}$ is the average value of the thermal image with maximum after normalized, and $T_{\text{normalization\_c}}$ – the value of the tumor center in the thermal image with maximum after normalized.

The effect of different tumor size and depth on the skin surface temperature signals under the given detection parameters is studied, which can provide a theoretical basis for the diagnosis of skin tumors using LP-ITWTT.

The effect of tumor radius, r, to maximum contrast c_{max}

The heat pulse power and its pulse width was set to 500 W and 120 seconds, repectively. The analysis time is 200 seconds. Figure 4 shows the maximum contrast c_{max} *vs.* different tumour radius, *r.* From fig. 4, it can be seen that, the greater the radius of tumor, tumor in the image conur more clear. According to eq. (5), the maximum contrast c_{max} was calculated when the tumor thickness is 0.7 mm, depth is 0.5 mm, and radius is 0.2 mm, 0.3 mm, 0.4 mm, 0.6 mm, 0.8 mm, and 1.0 mm, respectively. The maximum contrast, c_{max}, varies with tumor radius is shown in fig. 5. It shows that, for skin tumors with the same thickness and depth, larger radius of the tumor lead to greater maximum contrast, c_{max}, and this means that the tumors with larger

radius are more easily to be detected. From the above analysises, we can see that the tumor radius has a significant effect on the measurement parameter c_{max}.

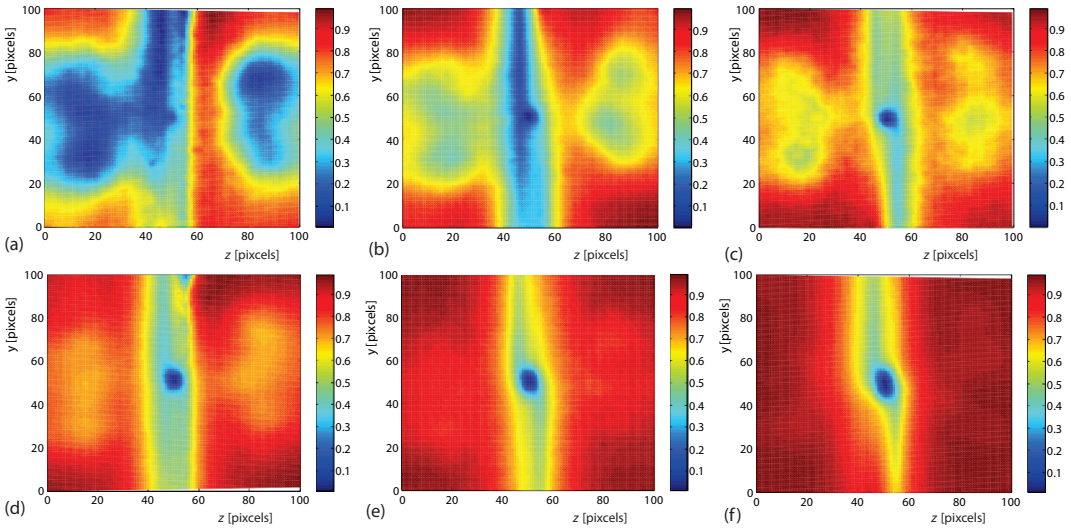

Figure 4. The thermal images with maximum c_{max} after normalized (h = 0.5 mm, l = 0.7 mm); (a) r = 0.2 mm (b) r = 0.3 mm (c) r = 0.4 mm, (d) r = 0.6 mm (e) r = 0.8 (f) r = 1.0 mm

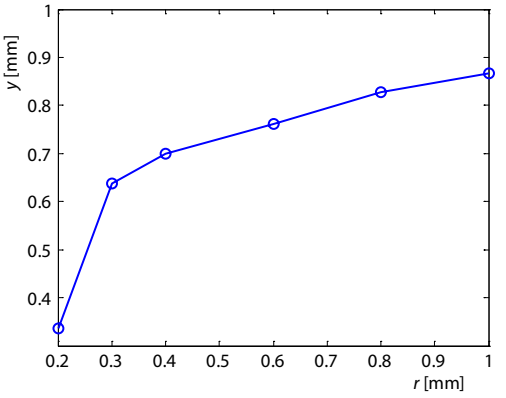

Figure 5. The maximum contrast c_{max} varies with tumor radius r (h = 0.5 mm, l = 0.7 mm)

The effect of tumor depth, h, to maximum contrast c_{max}

The heat pulse power and its pulse width are set to 500 W and 120 seconds, repectively. The analysis time is 200 seconds. Figure 6 shows the maximum contrast c_{max} *vs.* different tumour depth h. From fig. 6, it can be seen that, the greater the depth of tumor, tumor in the image conur more obscure. According to eq. (5), the maximum contrast, c_{max}, is calculated when the tumor thickness is 0.7 mm, radius is 0.5 mm, and depth is 0.1 mm, 0.15 mm, 0.35 mm, 0.45 mm, 0.6 mm, and 0.75 mm, respectively. The maximum contrast, c_{max}, varies with tumor depth, h, is shown in fig. 7. It can be seen that, for skin tumors with the same thickness and radius, larger depth of the tumor leads to smaller maximum contrast, c_{max}, and makes the tumor detection more difficult. The above analysis shows that tumor depth also has a significant effect on the measurement parameter, c_{max}.

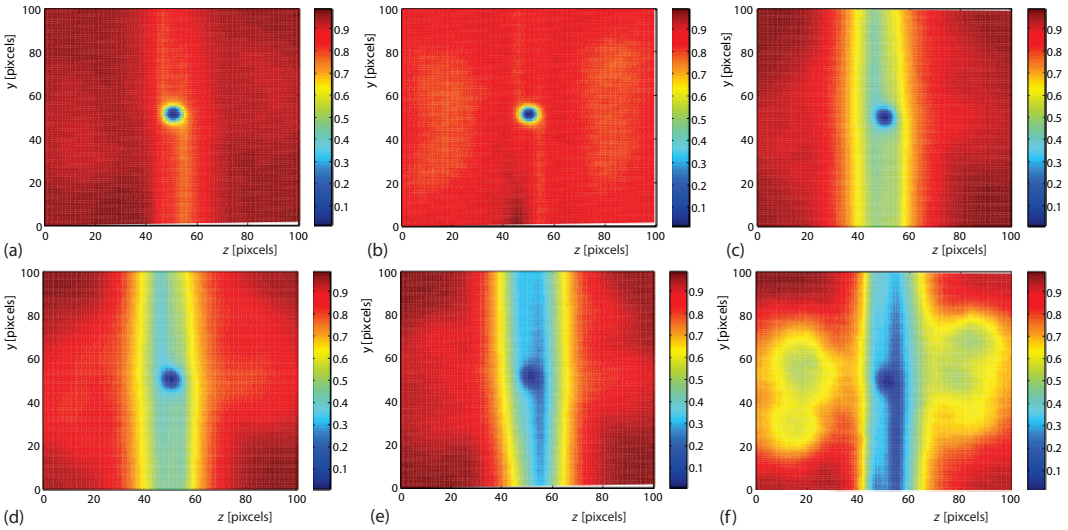

Figure 6. The thermal images with maximum, c_{max}, after normalized, r = 0.5 mm, l = 0.7 mm; (a) h = 0.1 mm (b) h = 0.15 mm (c) h = 0.35 mm, (d) h = 0.45 mm (e) h = 0.6 mm (f) h = 0.75 mm

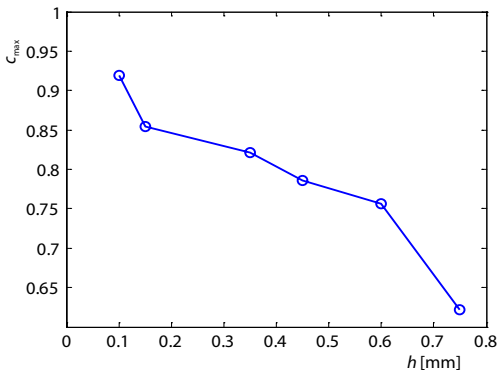

Figure 7. The maximum contrast c_{max} varies with tumor depth h (r = 0.5 mm, l = 0.7 mm)

The effect of tumor thickness, l, to maximum contrast c_{max}

The heat pulse power and its pulse width are set to 500 W and 120 seconds, repectively. The analysis time is 200 seconds. Figure 8 shows the maximum contrast *vs.* different tumour thickness, l. Figure 8 shows that, with greater thickness, tumor in the image conur more clear. The maximum contrast, c_{max}, varies with tumor thickness, l, is shown in fig. 9. With the same radius and depth, larger thickness of the tumor lead to greater maximum contrast c_{max}, which means it is more easily to be detected. From the above analysis, the tumor thickness also has an effect on the measurement parameter c_{max}.

Conclusion

The skin tumor detection using long-pulsed infrared thermal wave testing technology had been carried out. The working principle of long-pulsed infrared thermal wave testing technology was described. The 3-D thermal model for skin tumor using long-pulsed infrared thermal wave testing tech nology was established and calculated. It is shown that there are temperature differences between the normal regions and abnormal regions. The maximum contrast c_{max} is used to define the detection ability of tumors.

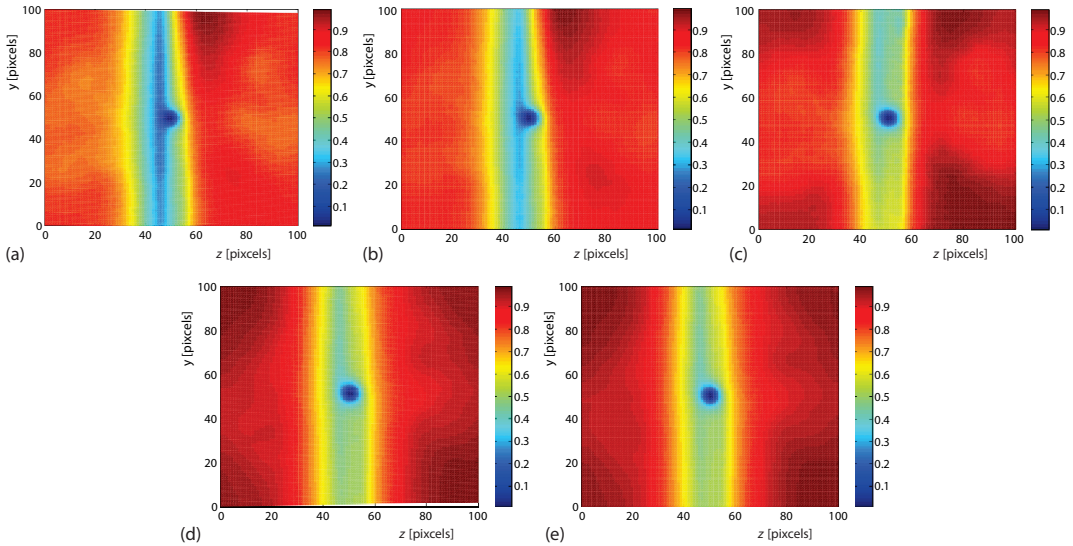

Figure 8. The thermal images with maximum c_{max} after normalized (r = 0.5 mm, h = 0.35 mm); (a) l = 0.2 mm (b) l = 0.3 mm (c) l = 0.4 mm, (d) l = 0.7 mm, and (e) l = 0.8 mm

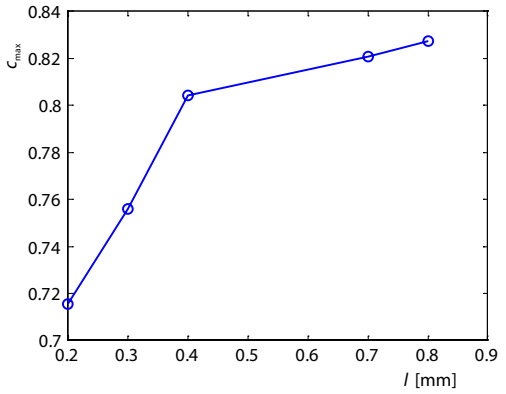

Figure 9. The maximum contrast c_{max} varies with tumor thickness l (r = 0.5 mm, h = 0.35 mm)

Acknowledgment

The authors thank doctors and experts in our hospitals for their diagnosis and research on tumors and cancer, which provides clinical guidance for the research of this paper.

Nomenclature

c – specific heat, [Jkg^{-1}K^{-1}]
q_b – heat transfer between the blood and biological tissues, [Wm^{-3}]
q_m – metabolic heat generation, [Wm^{-3}]
h_f – convective heat transfer coefficient, [Wm^{-2}K^{-1}]
$Q(t)$ – long pulsed heat flux, [W]
T_a – ambient temperature, [K]
T_c – core body temperature, [K]

Greek symbols

λ_x, λ_y, λ_z – thermal conductivities of tissue in the x-, y-, and z-directions, [Wm^{-1}K^{-1}]
ρ – density, [kgm^{-3}]

References

[1] Araujo, M. C., *et al.*, Interval Symbolic Feature Extraction for Thermography Breast Cancer Detection, *Expert Systems with Applications*, *41* (2014), 15, pp. 6728-6737

[2] Zhao, J., *et al.*, Using Raman Spectroscopy to Detect and Diagnose Skin Cancer In Vivo, *Dermatologic Clinics*, *35* (2017), 4, pp. 495-498
[3] Esteva, A, *et al.*, Dermatologist-Level Classification of Skin Cancer with Deep Neural Networks, *Nature*, *542* (2017), 7639, pp. 115-118
[4] Narayanamurthy, V., *et al.*, Skin Cancer Detection Using Non-invasive Techniques, *Rsc Advances*, *49* (2018), 8, pp. 28095-28130
[5] Godoy, S. E., *et al.*, Dynamic Infrared Imaging for Skin Cancer Screening, *Infrared Physics and Technology*, *70* (2015), pp. 147-152
[6] Hagerlind, E., *et al.*, Near Infrared and Skin Impedance Spectroscopy – A Possible Support in the Diagnostic Process of Skin Tumours in Primary Health Care, *Skin Research & Technology*, *21* (2015), 4, pp. 493-499
[7] Bhowmik, A., *et al.*, Suitability of Frequency Modulated Thermal Wave Imaging for Skin Cancer Detection – A Theoretical Prediction, *Journal of Thermal Biology*, *51* (2015), July, pp. 65-82
[8] Yang, X., General Fractional Calculus Operators Containing the Generalized Mittag-Leffler Functions Applied to Anomalous Relaxation, *Thermal Science*, *21* (2017), 2, pp. 196
[9] Wissler, E. H., Pennes' 1948 Paper Revisited, *Journal of Applied Physiology*, 85 (1998), 1, pp. 35-41
[10] Kashcooli, M., *et al.*, Heat Transfer Analysis of Skin During Thermal Therapy Using Thermal Wave Equation, *Journal of Thermal Biology*, *64* (2017), 2, pp. 1-7

Paper submitted: August 23, 2018
Paper revised: November 19, 2018
Paper accepted: February 29, 2019